ICE NECK FRACTURE EXPERIMENTS

A. Luque[1], J. Aldazabal[1], A. Martín–Meizoso[1], J.M. Martínez–Esnaola[1], J. Gil Sevillano[1], R.S. Farr[2], A. Hoodle[3]

[1] CEIT and Tecnun (University of Navarra). Paseo Manuel Lardizábal 15, 20018 San Sebastián. Spain.
E–mail: aluque@ceit.es. Phone: +34 943212800. Fax: +34 943213076.
[2] Unilever R&D. Olivier van Noortlaan 120, AT3133 Vlaardingen. The Netherlands.
[3] Unilever R&D, Colworth House. Sharnbrook, MK44 1LQ Bedford. United Kingdom.

ABSTRACT

This paper summarizes the results of fracture experiments carried out on ice necks at –18 ºC. The neck geometry is a meniscus. This shape is attained freezing water between a flat plate and a spherical probe which are moved apart during the tensile test. Two types of fracture are observed: adhesive fracture and cohesive fracture. Adhesive failure occurs by propagation of a crack between the sample and one of the parts which "attaches" the sample to the equipment. Cohesive failure takes place by propagation of an internal crack within the solidified water. Each fracture behaviour is characterised by a different fracture stress. In this work, we also try to estimate the Young's modulus of ice.

KEY WORDS: Tensile test, ice, fracture stress, adhesive failure, cohesive failure, Young's modulus.

1. ICE MECHANICAL PROPERTIES

Mechanical properties of ice are relevant to those natural and artificial environments in which liquid water and low temperatures can be found at the same time. Some illustrative examples of this are the breakup of glaciers and avalanche event prediction (Glaciology) or the icing of structures in cold climates (Civil, Naval and Aeronautical Engineering). In Food Science, this topic is of interest to the preservation of optimal consumption conditions of frozen foods: microstructural details (ripening of ice particles and formation and growth of ice–ice necks) affect the sensory properties which are eventually felt by consumers.

These are some of the mechanical properties of ice:

- Monocrystalline hexagonal I_h ice shows a moderate anisotropy with C_{11} = 13.7 GPa, C_{12} = 7.0 GPa, C_{13} = 5.6 GPa, C_{33} = 14.7 GPa and C_{44} = 3.0 GPa (3–axis coincides with the c_{Ih} direction) [1,2].
- For randomly–oriented ice polycrystals, values of Young's modulus, E, between 9.0 and 9.5 GPa are reported, and Poisson's ratio, ν, ranges from 0.3 to 0.325 [1–5].
- The inelastic behaviour of ice is also markedly anisotropic. The critical resolved shear stress for non–basal slip is several times greater than that for basal slip [1–4]. This leads to the build–up of internal stresses at grain–size scale which can initiate cracks. Ice exhibits macroscopically ductile or brittle behaviour depending on the tolerance to these cracks [6].
- Tensile strength, σ_f, of polycrystalline ice ranges from 0.7 MPa to 3.1 MPa [5,6], between –20 ºC and –10 ºC, with the typical scatter associated to fracture measurements.
- Ice fracture toughness, K_{Ic}, ranges from 50 kPa√m to 110 kPa√m [1,2,5,7,8].

In this work, we carry out tensile tests of ice samples at –18 ºC, in order to study the fracture behaviour of ice particles when they have joined and form a neck. As the implementation of such an experiment can be difficult [9], the chosen geometry is a meniscus of solidified water formed between the two parts of a tensile tester which are moved apart during the experiment.

2. EQUIPMENT AND PROCEDURE

The fracture tests are performed in an Instron 4501 tensile tester. It is provided with a load cell of 100 N and it can carry out the tests in either force or displacement control.

The generation of ice necks and the experiments take place within a cold chamber which is kept at –18 ºC. The temperature control is also provided by Instron: an income flow of cold N_2 gas to the chamber is established to reach the target temperature. However, the pump of gas is discontinuous (~10 s) and thus, the temperature control may not be very precise.

In order to perform these experiments, a flat plate and a spherical probe of Ø5 mm are introduced into the cold chamber and clamped to the fixed part and to the crosshead, respectively. Then, we let these two parts freeze. Before generating the samples, an ice layer is grown on the spherical probe with the help of a pipette (Figure 1.a). Finally, the probes approach one another until they are 1 mm or 2 mm away. In that moment, load and displacement signals are set to zero. Next, a very small amount of water is placed between the probes with the help of a syringe (Figure 1.b). Only 5 mm^3 or 10 mm^3 are enough to form a meniscus (Figure 1.c).

Finally, the experiment can start and is carried out under displacement control. The test can be divided into two parts: the cooling step and the loading step. During

cooling, the sample is kept at –18 ºC for 2 min and the crosshead does not move. During the loading step, the crosshead starts to move at a rate of 0.1 mm/min and the loading of the sample occurs.

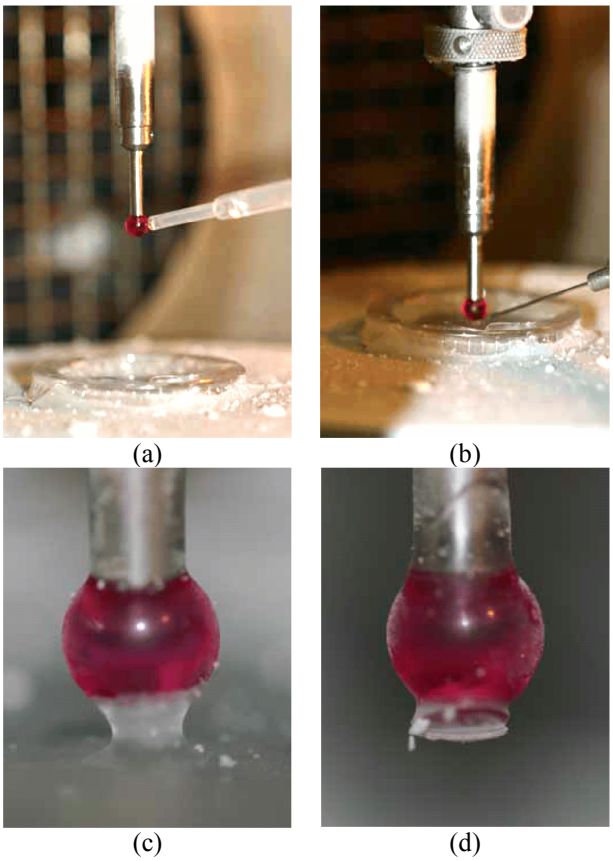

Figure 1. (a) *Preparation of the Ø5 mm spherical probe.* (b) *Generation of an ice neck between the probes.* (c) *Ice neck (meniscus) before tensile test.* (d) *Ice neck after fracture (cohesive failure).*

3. RESULTS

Although the (deliberate) loading of the sample takes place during the loading step, some of the samples broke during the cooling step. This can be understood if we recall that the liquid meniscus freezes during this step. Due to the displacement control of the equipment, the crosshead is impeded to move during cooling. Nevertheless, the meniscus contracts during its solidification. Therefore, a net tensile load is applied on the meniscus and that is registered by the equipment. Whether or not the load introduced during the cooling step is enough to break the neck depends on its production and solidification. If fracture does not take place during the first step of the experiments, then it occurs during the second part, as expected (Figure 1.d).

Figure 2.a shows the load *vs.* time $F - t$ curves of the menisci that broke during the cooling step. Figure 2.b shows the load *vs.* displacement $F - \Delta L$ curves of the necks that broke during the loading step.

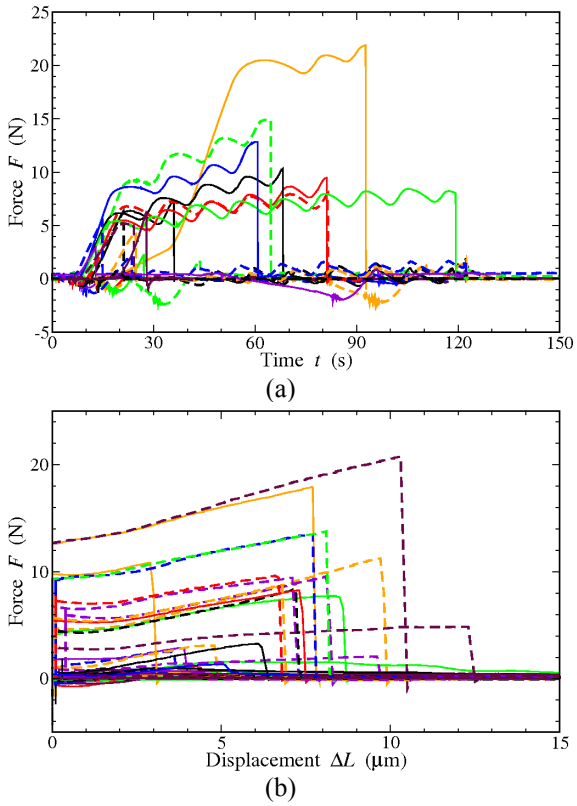

Figure 2. (a) *Load – time curves corresponding to necks broken during cooling.* (b) *Load – displacement curves corresponding to necks broken during loading.*

Apart from the classification of broken necks in terms of the moment of their actual fracture, they can also be classified in terms of the fracture type that they exhibit. A simple inspection permits classifying fracture into adhesive and cohesive. Adhesive failure corresponds to a crack appearing between ice and the spherical probe (Figure 3.a), whereas cohesive failure corresponds to a crack propagating through the ice (Figure 3.b).

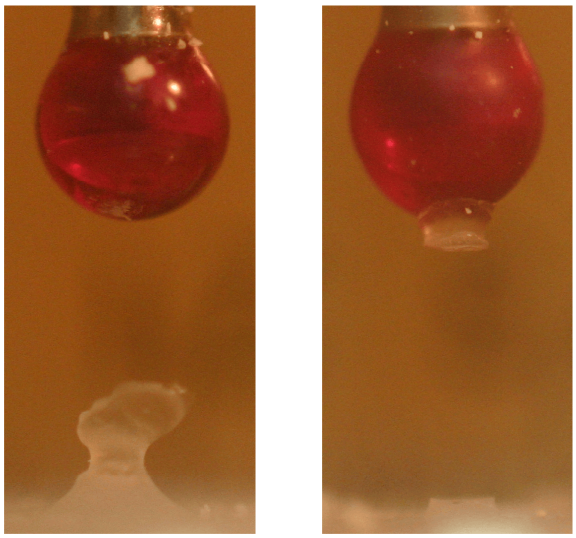

Figure 3. Different types of fracture observed: (a) *adhesive failure and* (b) *cohesive failure.*

Nevertheless, this new division is independent of the aforementioned one. This is: the two types of failure were observed both during cooling and during loading.

From the $F - \Delta L$ curves (Figure 2.b), we can calculate the ice Young's modulus and the value of fracture stress, σ_f, of both adhesive and cohesive failure. However, from the $F - t$ curves (Figure 2.a), we can only calculate σ_f The obtained values of σ_f and E are summarized in the following sections.

3.1. Fracture stress

The first approach to obtain the fracture stress is simply to calculate the average stress in the neck, σ_{ave}, *i.e.* the applied force, F, divided by the section, A, of the neck. However, this value must be corrected by a term, namely f_{corr}, in order to take into account the triaxiality contribution to σ_f, such that $\sigma_f = f_{corr} \cdot \sigma_{ave}$. This factor has been computed using Abaqus and considering different neck sizes, X, neck curvatures, ρ, and neck lengths, L_{neck}. The geometry employed in Abaqus to obtain this factor mimics the meniscus geometry, as shown in Figure 4.

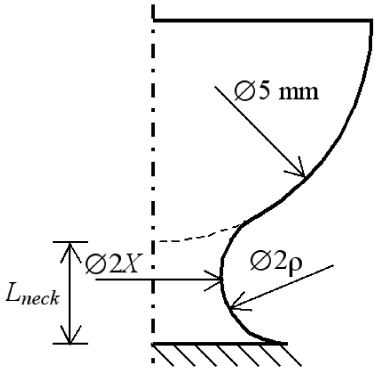

Figure 4. Geometry of the neck simulated in Abaqus for the estimation of the triaxiality correction factor, f_{corr}.

Within the analyzed range of X/ρ, which contains the X/ρ values of the experiments, the correction factor can be fitted to

$$f_{corr} = 1.33 + 0.18 \ln(X/\rho) \qquad (1)$$

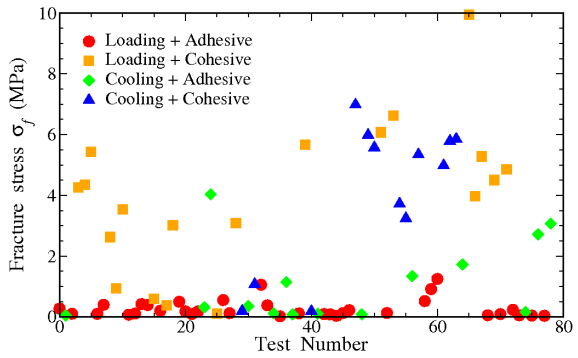

Figure 5. Fracture stress, σ_f, associated to each neck.

Figure 5 shows the fracture stress associated to these experiments. The colour/shape code indicates the moment and the type of failure. The mean fracture stresses are summarized in Table 1.

Table 1. Mean values of fracture stress, σ_f, and Young's modulus, E, of the observed failure types.

	σ_f (MPa)	E (MPa)
Loading + Adhesive	0.3 ± 0.3	70 ± 50
Loading + Cohesive	4 ± 2	200 ± 100
Cooling + Adhesive	1 ± 1	
Cooling + Cohesive	4 ± 2	

We can observe that the ice necks showing cohesive failure yield a mean fracture stress of approximately 4 MPa. The obtained value of σ_f is slightly higher than those reported in the literature (0.7 MPa – 3.1 MPa [5]). Nevertheless, the scatter associated to these results is high and, thus, the differences are not really relevant.

In relation with adhesive failure, we can observe more differences between the ice samples broken during cooling and those broken during loading (on average, 1 MPa *vs.* 0.3 MPa). In both cases, the scatter is high. The scatter is such that a possible result for σ_f is zero. That would mean that there is very small adhesion between the surfaces. This would indicate that more attention should have been paid during the surface preparation and the sample production. This could also have reduced the number of adhesive events.

It is interesting to analyse these fracture stress results in terms of Weibull distribution [10]

$$P(\sigma_f) = 1 - \exp[-(\sigma_f / \sigma_{f0})^k] \qquad (2)$$

where k is the shape parameter and σ_{f0} is the scale parameter, which corresponds to the value for which the ~63% of the measured fracture stresses is below σ_{f0}. For this purpose, all the results of adhesive failure and those of cohesive failure have been grouped in two different data sets, as shown in Figure 6.

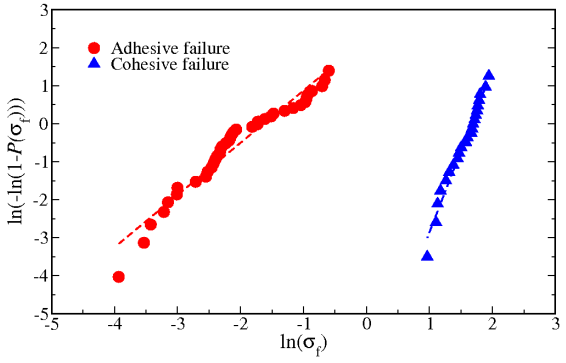

Figure 6. Weibull distribution of fracture stress, σ_f, associated to the observed fracture types.

For adhesive fracture, we have obtained a shape parameter of 1.4 and a size parameter of 0.20 MPa. Nevertheless, the fit is not as good as for the cohesive fracture, for which the shape parameter increases up to 4.3 and the size parameter is approximately 5.3 MPa. This is 25 times bigger than the value obtained for adhesive failure, a similar result if we consider the mean values of σ_f. This is in good agreement with the scatter shown in Table 1, which indicates that the estimates for the fracture stress for cohesive failure are more reliable than those for adhesive failure. Some authors [9,11] attribute this difference to the existence of a liquid–like layer between the surfaces. This layer, whose existence may be possible from a thermodynamical point of view, represents an easily separable zone. Thus, failure can proceed preferentially through that layer. However, the existence of this layer could not be demonstrated experimentally in these samples. Finally, the shape parameter value for cohesive failure obtained in this work is of the same order as the values reported in the literature, which range between 3 and 5 [5,8].

3.2. Young's modulus

If we now consider the deformation undergone by the ice necks during the cooling step, we can estimate the value of Young's modulus, E. We have already mentioned that the geometry of the sample induces stress triaxiality during the tensile test. The axial stress is not uniform through the neck, nor is the axial strain. As a first approximation, we are going to calculate E as

$$E = \frac{\sigma_{ave} - \sigma(0)}{\varepsilon_{ave}} = \frac{F_{max} - F(0)}{A}\frac{L_{neck}}{\Delta L} \qquad (3)$$

where $\sigma(0)$ is the average axial stress at the beginning of the loading step, calculated from the load at that particular instant, $F(0)$, ε_{ave} is the uniform axial strain and ΔL is the change in the "length" of the neck. The change of neck section during the tensile test is neglected. Figure 7 presents the values of Young's modulus along the axial direction, obtained from these experiments. Obviously, no estimations for E can be obtained from the necks broken during the cooling step ($\varepsilon = 0$). Table 1 also summarizes the mean values of Young's modulus for the different failure types.

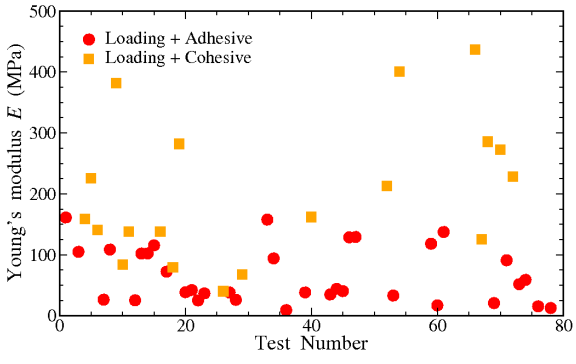

Figure 7. Young's modulus, E, associated to each neck.

For the adhesive failure, the average Young's modulus is 70 MPa, whereas for the cohesive failure, it is 200 MPa. There is a relevant scatter for this parameter, as shown in Figure 7. Besides, the difference in terms of E for the two fracture types is not as big as for σ_f. This is in line with what we expected, as the value of ice Young's modulus should be independent of the nature of the fracture occurred.

However, the values of this work are very far from the reported value for polycrystalline ice, namely 9.33 GPa [1,2,5]. This big difference may indicate that a certain ice softening process is taking place. It could simply be the inherent softness of just–solidified ice [5] or the aforementioned liquid–like layer surrounding ice particles. Both phenomena would yield a decrease of E in "fresh" ice with respect to "old" bulk ice. Nevertheless, the combination of temperature and time should avoid the effect of the liquid layer, if such effect exists.

A comment should be made regarding the parameters appearing in Equation 3. Forces and neck geometry seem correct on the basis of the fracture stress values that we have obtained. However, there is some uncertainty in the neck elongation, ΔL. Just note that to get σ_{ave} = 4 MPa with E = 10 GPa and L_{neck} = 1 mm, ΔL should be 400 nm, whereas the registered values are, at least, one order of magnitude bigger. Therefore, these values may not simply be the ice elongation, but a combination of the elongations of the neck and of some part of the machine of lower stiffness, K_{mach} (compared with ice; this is, $K_{mach} < K_{ice}$). A schematic of the system is depicted in Figure 8.

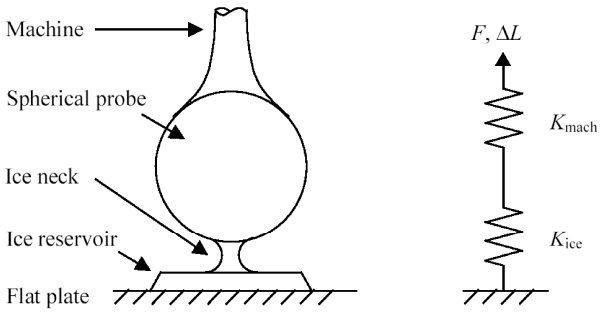

Figure 8. Schematic of the system proposed for explaining the "soft ice".

This configuration yields

$$\Delta L = \Delta L_{ice} + \Delta L_{mach} \qquad (4)$$

where the (known) value of ΔL is decomposed into two terms, one corresponding to ice and another one corresponding to the softer part of the machine. On the other hand, while the stiffness of this softer part is unknown, the stiffness of ice can be calculated as $K_{ice} = EA/L_{neck}$. As the springs depicted in Figure 8 are connected in series, the applied force is undergone by both springs. Assuming the applicability of Hooke's

law, together with Equation 4, we get

$$\frac{\Delta L}{F} = \frac{1}{K_{mach}} + \frac{1}{E}\frac{L_{neck}}{A} \qquad (5)$$

Therefore, if we plot $\Delta L/F$ *vs.* L_{neck}/A for our experiments, we can, in principle, obtain the compliance of the softer part of the machine, $1/K_{mach}$, as L_{neck}/A tends to 0, and the "real" ice Young's modulus, E, as the inverse of the slope of the linear fit given by Equation 5. Figure 9 shows the dependence of $\Delta L/F$ on L_{neck}/A, for the cohesive fractures during loading.

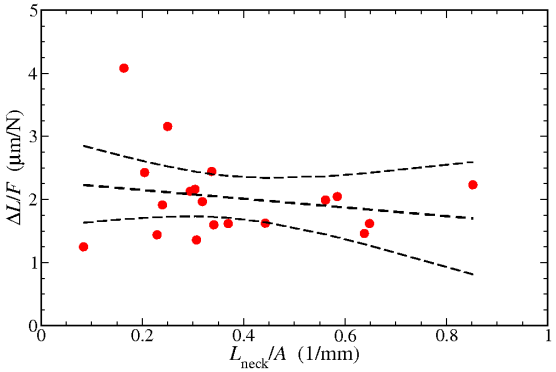

Figure 9. $\Delta L/F$ vs. L_{neck}/A plot of the necks broken during the loading step showing cohesive fracture. The linear fit is shown, as well as the 95% confidence interval for the given linear fit [12].

According to the results shown in Figure 9, the stiffness of the softer part of the machine would be $K_{mach} \approx 450$ kN/m and the value of E would be negative. However, the correlation coefficient of this linear fit is very poor (only 20%). This is: we can hardly say that a line fits our points. Anyway, if we consider the confidence interval of the fit, the value of Young's modulus can be as small as ~1 GPa, which is still one order of magnitude smaller than the real elastic modulus of polycrystalline ice. Nevertheless, note that the experimental results are somewhat concentrated around 0.3 mm^{-1} and 2 μm/N, but, at the same time, there are some values of up to 0.85 mm^{-1} and 4 μm/N. The calculation of the inverse of the slope of a new linear fit which drops out these extreme values would yield a much more accurate value of ~4 GPa, still lower than the reported values but now only two and a half times as small as those.

4. CONCLUSIONS

The mechanical behaviour of ice necks has been studied through an equivalent configuration, namely a meniscus of solidified water.

We have observed that fracture can occur prior to the loading of the samples, due to the contraction of water during solidification. Fracture can also take place during sample loading, as expected.

Independently of when fracture happens, two types of failure have been identified. The first type is an adhesive failure, in which a crack propagates between the ice meniscus and one of the attaching surfaces. The fracture stress associated to this type of failure is between 0.3 MPa and 1 MPa. The second type of failure that we have identified is the cohesive failure. In this case, the crack propagates through the middle of the samples. The fracture stress associated to this fracture type is, on average, 4 MPa. The scatter associated to these measurements is rather big. Nevertheless, these values are similar to the values reported in the bibliography. Besides, adhesive fracture and cohesive fracture have yielded different results in terms of Weibull shape parameter (1.4 *vs.* 4.3).

We have also tried to calculate the elastic modulus of ice from the necks broken during the loading step. The results are similar for adhesive failure and cohesive failure (75 MPa vs. 230 MPa, respectively). However, the obtained values of Young's modulus are, at least, one order of magnitude smaller than those reported in the literature. This has been justified by the presence of a more compliant part in the experimental set–up.

ACKNOWLEDGEMENTS

The authors would like to thank Unilever R&D Colworth (UK), for the support of this research, and to Ian Burns (Unilever R&D). A. Luque would also like to thank the Spanish Ministry of Education and Science and the European Social Fund for the funding and co–funding, respectively, of his contract (Torres Quevedo Programme).

REFERENCES

[1] Petrenko, V.F. and Whitworth, R.W., Physics of Ice, Oxford University Press, Oxford (UK), 2002.

[2] Schulson, E.M. and Duval, P., Creep and fracture of ice, Cambridge University Press, Cambridge (UK), 2009.

[3] Schulson, E.M., "The structure and mechanical behavior of ice", JOM, 51, 1999, 21–27.

[4] Mansuy, P., Contribution à l'étude du comportement viscoplastique d'un multicristal de glace: hétérogénéité de la déformation et localisation, expériences et modèles, Ph.D. thesis, University of Joseph Fourier – Grenoble I, San Martin d'Hères (France), 2001, 3–8.

[5] Petrovic, J.J., "Mechanical properties of ice and snow", J. Mat. Sci., 38, 2003, 1–6.

[6] Currier, J.H. and Schulson, E.M., "The tensile strength of ice as a function of grain size", Acta Metallurgica, 30, 1982, 1511–1514.

[7] Tromans, D. and Meech, J.A., "Fracture toughness and surface energies of covalent minerals: theoretical estimates", Minerals Eng., 17, 2004, 1–15.

[8] Kamio, Z., Matsushita, H. and Strnadel, B., “Statistical analysis of ice fracture characteristics”, Eng. Fracture Mechanics, 70, 2003, 2075–2088.
[9] Fan, X., Ten, P., Clarke, C.J., Bramley, A.S. and Zhang Z., “Direct measurement of the adhesive force between ice particles by micromanipulation”, Powder Technology, 131, 2003, 105–110.
[10] Hajek, J., Probability in science and engineering, Academic Press, New York (USA), 1967.
[11] Andrews, E.H. and Lockington, N.A., “The cohesive and adhesive strength of ice”, J. Mat. Sci., 18, 1983, 1455–1465.
[12] Ríos, S., Métodos estadísticos, Ibérica, Madrid (Spain), 1965.